2012

A functional description of CymA, an electron-transfer hub supporting anaerobic respiratory flexibility in *Shewanella*

Sophie J. Marritt
University of East Anglia

Thomas G. Lowe
University of East Anglia

Jordan Bye
University of East Anglia

Duncan G. G. Mcmillan
University of Leeds

Liang Shi
Pacific Northwest National Laboratory, liang.shi@pnl.gov

See next page for additional authors

BJ www.biochemj.org

Biochem. J. (2012) **444**, 465–474 (Printed in Great Britain) doi:10.1042/BJ20120197

online data

A functional description of CymA, an electron-transfer hub supporting anaerobic respiratory flexibility in *Shewanella*

Sophie J. MARRITT*, Thomas G. LOWE*, Jordan BYE*, Duncan G. G. McMILLAN†, Liang SHI‡, Jim FREDRICKSON‡, John ZACHARA‡, David J. RICHARDSON*, Myles R. CHEESMAN*, Lars J. C. JEUKEN† and Julea N. BUTT*[1]

*Centre for Molecular and Structural Biochemistry, School of Chemistry and School of Biological Sciences, University of East Anglia, Norwich NR4 7TJ, U.K., †Institute of Membrane and Systems Biology, Centre for Molecular Nanoscience, School of Physics and Astronomy, University of Leeds, Leeds LS2 9JT, U.K., and ‡Pacific Northwest National Laboratory, Richland, WA 99352, U.S.A.

CymA (tetrahaem cytochrome *c*) is a member of the NapC/NirT family of quinol dehydrogenases. Essential for the anaerobic respiratory flexibility of shewanellae, CymA transfers electrons from menaquinol to various dedicated systems for the reduction of terminal electron acceptors including fumarate and insoluble minerals of Fe(III). Spectroscopic characterization of CymA from *Shewanella oneidensis* strain MR-1 identifies three low-spin His/His co-ordinated *c*-haems and a single high-spin *c*-haem with His/H_2O co-ordination lying adjacent to the quinol-binding site. At pH 7, binding of the menaquinol analogue, 2-heptyl-4-hydroxyquinoline-*N*-oxide, does not alter the mid-point potentials of the high-spin (approximately -240 mV) and low-spin (approximately -110, -190 and -265 mV) haems that appear biased to transfer electrons from the high- to low-spin centres following quinol oxidation. CymA is reduced with menadiol ($E_m = -80$ mV) in the presence of NADH ($E_m = -320$ mV) and an NADH–menadione (2-methyl-1,4-naphthoquinone) oxidoreductase, but not by menadiol alone. In cytoplasmic membranes reduction of CymA may then require the thermodynamic driving force from NADH, formate or H_2 oxidation as the redox poise of the menaquinol pool in isolation is insufficient. Spectroscopic studies suggest that CymA requires a non-haem co-factor for quinol oxidation and that the reduced enzyme forms a 1:1 complex with its redox partner Fcc_3 (flavocytochrome c_3 fumarate reductase). The implications for CymA supporting the respiratory flexibility of shewanellae are discussed.

Key words: cytochrome, electron paramagnetic resonance (EPR), electron transfer, magnetic circular dichroism (MCD), mineral respiration, quinol dehydrogenase.

INTRODUCTION

The *Shewanella* genus of γ-proteobacteria comprises a diverse group of facultative anaerobes [1]. Their ability to couple the oxidation of various carbon sources to the reduction of a broad range of terminal electron acceptors imparts a respiratory flexibility that allows colonization of varied, and changeable, marine and freshwater environments. *Shewanella oneidensis* strain MR-1 is the most extensively characterized of the shewanellae. It can use O_2, fumarate, nitrate, thiosulfate, sulfite, elemental sulfur and trimethylamine *N*-oxide as terminal electron acceptors. These substrates enter the periplasm where their reduction is catalysed by dedicated enzymes homologous with well-characterized reductases found in many proteobacteria. However, *S. oneidensis* MR-1 is also capable of using particulate DMSO and the Fe(III) and Mn(III/IV) contained in oxide and phyllosilicate minerals as terminal electron acceptors. Reduction of these particulates occurs in the extracellular matrix catalysed by novel multihaem cytochromes whose structural and biochemical properties are beginning to emerge [2–6]. Electrons are delivered to the extracellular matrix from the periplasm by a porin–cytochrome complex that spans the outer membrane and has a biochemistry of significant biotechnological impact. The activity of the complex can be harnessed to pass electrons to the anode of microbial fuel cells and to facilitate the bioremediation of contaminated sediments by converting soluble radionuclides such as U(VI) and Tc(VII) into reduced less-soluble forms [1,7].

Regardless of the nature and location of the terminal electron acceptor, redox cycling of Q (quinone) and its two electron reduced form QH_2 (quinol) in the cytoplasmic membrane is key to respiratory energy conservation in *S. oneidensis* MR-1 [8–10]. Electrons from the oxidation of organic electron donors drive the reduction of Q to QH_2 after which these electrons are directed to the periplasm through the action of QH_2 dehydrogenases such as CymA (tetrahaem cytochrome *c*). CymA is a member of the NapC/NirT family of QH_2 dehydrogenases and essential for the respiratory reduction of nitrate, nitrite, fumarate, DMSO, soluble complexed forms of Fe(III) and extracellular particulate substrates [11–15]. These enzymes, which in proteobacteria are more phylogenetically widespread than the cytochrome bc_1 complex, possess a single N-terminal transmembrane helix with a globular haem-binding domain that protrudes into the periplasm for interaction with terminal reductases. At present, the only structures available for NapC/NirT homologues are of the homodimer NrfH (cytochrome *c* nitrite reductase small subunit) in the QH_2–nitrite oxidoreductase complex $(NrfH)_2(NrfA)_4$ from *Desulfovibrio vulgaris* [16,17]. Haem I is located in the globular domain in proximity to the QH_2-binding site and haems II and III are positioned to relay electrons from haem I to the point of contact with the NrfA nitrite reductase at haem IV (haems are numbered in order of the CxxCH binding motifs in the primary structure). The axial ligands to haems II and III are provided by two histidine ligands as is typical for multihaem cytochromes; however, haems I and IV have unusual axial ligation. Haem I

Abbreviations used: CymA, tetrahaem cytochrome *c*; DDM, dodecyl maltoside; Fcc_3, flavocytochrome c_3 fumarate reductase; HQNO, 2-heptyl-4-hydroxyquinoline-*N*-oxide; LB, Luria–Bertani; LMCT, ligand-to-metal charge-transfer; MALDI–TOF-MS, matrix-assisted laser-desorption ionization–time-of-flight MS; MCD, magnetic circular dichroism; menadione, 2-methyl-1,4-naphthoquinone; NaHepes, sodium salt of Hepes; NrfH, cytochrome *c* nitrite reductase small subunit; Q, quinone; QH_2, quinol; SHE, standard hydrogen electrode.

[1] To whom correspondence should be addressed (email j.butt@uea.ac.uk).

is penta-co-ordinate with proximal ligation by methionine rather than the usual histidine from the CxxCH haem-binding motif. The proximal ligand of haem IV is histidine from its CxxCH binding motif. However, the distal ligand is provided by lysine from another subunit, namely, the NrfA nitrite reductase.

The specificity of the QH_2 dehydrogenase–reductase partnership exemplified by NrfHA is typical for pathways dependent on NapC/NirT family members that can be characterized solely by their genomic context [18–22]. In contrast, *cymA* is an orphan gene in *S. oneidensis* MR-1 that is expressed constitutively, but up-regulated when fumarate or an electrode serve as the terminal electron acceptor [11,23,24]. Transient formation of CymA–reductase complexes would facilitate the distribution of electrons from QH_2 to various terminal electron acceptors such that covalent linkage between CymA and its redox partners seems unlikely. Certainly *Shewanella frigidimarina* CymA, like other NapC/NirT family members and in contrast with *D. vulgaris* NrfH, can be purified in the absence of a terminal reductase suggesting that association with the periplasmic redox partner is not essential for stability [25–28].

Given the high sequence identity, typically >73 %, displayed by CymA within the clade of *Shewanella* it is likely that these enzymes have similar structures and mechanisms for QH_2 oxidation. Accordingly, the haems in the soluble globular domain of *S. oneidensis* MR-1 CymA and the full-length CymA from *S. frigidimarina* have midpoint potentials (E_m) between approximately + 10 and − 260 mV compared with SHE (standard hydrogen electrode) [26,29,30]. Spectroscopic analysis of *S. frigidimarina* CymA by Richardson and colleagues led to the proposal that each of the four haems have His/His ligation [26]. There are sufficient conserved histidine residues in the sequence to accommodate this pattern of ligation, but it has significant implications with regard to presenting a unified mechanism for QH_2 oxidation across the NapC/NrfH family. Whereas QH_2 oxidation is proposed to occur at penta-co-ordinate haem I with methionine ligation in NrfH, it would appear to be catalysed by a hexa-co-ordinate His/His-ligated haem in CymA. Alternatively QH_2 binding to CymA may induce a change of ligation at the QH_2 oxidizing haem perhaps driving it to a penta-co-ordinate form. The latter scenario may change the spin-state and/or reduction potentials of the CymA haems and so the framework in which QH_2 oxidation is considered.

In *Shewanella* sp. during anaerobic growth when the activity of CymA is critical the QH_2 pool is dominated by menaquinols and methylmenaquinols ($E_m \sim -80$ mV) [15,31,32]. Consequently, we have applied a combination of spectroscopic methods and potentiometric titration to resolve structural, thermodynamic and kinetic properties of *S. oneidensis* MR-1 CymA in the absence and presence of two menaquinol analogues, namely, menadiol and HQNO (2-heptyl-4-hydroxyquinoline-*N*-oxide). We have also assessed the extent of CymA reduction that can be achieved in the absence and presence of a periplasmic redox partner Fcc_3 (flavocytochrome c_3 fumarate reductase). The results of the present study allow us to present a revised functional description of CymA that is relevant to the anaerobic respiratory flexibility of *Shewanella* sp.

EXPERIMENTAL

Purification of CymA and Fcc_3 from *S. oneidensis* MR-1

CymA was purified from *S. oneidensis* MR-1 as described previously for the purification of the enzyme from *S. frigidimarina* [26], with cultures grown micro-aerobically in LB (Luria–Bertani) medium at pH 7.5 supplemented with 50 mM DL-lactate. The low yields of CymA from these cells prompted construction of an overexpression strain as described below. Soluble Fcc_3 was purified from *S. oneidensis* MR-1 as described previously [33].

Construction of an overexpression system for CymA

The *cymA* gene (locus tag SO4591) of *S. oneidensis* MR-1 was cloned using the protocol described previously for overexpression of *Shewanella* multihaem cytochromes [34,35]. Briefly, the gene was amplified by PCR with primers 5′-CACC**TAA**GAAGGA-GATATACATCCC**ATG**AACTGGCGTGCACTATTTAAAC-3′ (*cymA* 1–25 bp; insertion sites are in bold) and 3′-GAGTGG-GGATAGGTTTTCCT-5′ (*cymA* 541–561 bp). The PCR product was cloned into a protein expression vector derived from pBAD202/D-TOPO (Invitrogen) to create the plasmid pLS167. Following verification by sequencing, pLS167 was transformed into *S. oneidensis* MR-1 cells to create an MR-1 strain LS447 maintained on LB medium plates containing 50 $\mu g \cdot ml^{-1}$ kanamycin.

Purification of recombinant CymA

Recombinant CymA was purified from membranes of *S. oneidensis* MR-1 strain LS447 grown at 30 °C in Terrific Broth adjusted to pH 7.5 and containing 50 $\mu g \cdot ml^{-1}$ kanamycin. Micro-aerobic growth was achieved by shaking 1 litre batch cultures in 2 litre conical flasks at 180 rev./min. Overexpression of *cymA* was induced by the addition of 1 mM arabinose during exponential growth at an attenuance of ~0.7 at 600 nm. Cells were harvested after a further 18 h of growth by centrifugation at 15000 ***g*** for 30 min at 4 °C, washed twice and resuspended in 100 mM NaHepes (sodium salt of Hepes) pH 7.5 buffer. Cell lysis was performed by two passages through a French Press at a pressure of 1000 psi (1 psi = 6.9 kPa). Membranes were pelleted by ultracentrifugation at 4000 rev./min at 4 °C with a Beckman 45Ti rotor in 100 mM NaHepes (pH 7.5), homogenized and washed twice in 100 mM NaHepes buffer containing 100 mM NaCl, 1 mM EDTA and protease inhibitors (Roche).

Membrane proteins were solubilized in 50 mM NaHepes (pH 7.5) containing 2 mM EDTA, protease inhibitors and 1 % (w/v) DDM (dodecyl maltoside) for 16 h at 4 °C, and insoluble material was removed by ultracentrifugation. Purification of CymA was then monitored by SDS/PAGE and electronic absorbance spectroscopy with all steps performed at 4 °C. Solubilized membrane proteins at approximately 20 mg $\cdot ml^{-1}$ were diluted 10-fold in 20 mM Tris/HCl and 1 mM EDTA (pH 8.8) and stirred into a slurry of DEAE Sepharose CL-6B anion-exchange medium (GE Healthcare). CymA was extracted by batch elution with increasing concentrations of NaCl in 20 mM Tris/HCl (pH 8.8) containing 0.05 % DDM. Elution with 130 mM NaCl isolated a fraction containing the majority of CymA that was concentrated by ultrafiltration over an Amicon YM30 membrane and then dialysed overnight against 20 mM NaHepes, pH 7. DDM was excluded from the dialysis buffer because the micelle size (50 kDa) and slow rate of detergent exchange between micelle and solution will result in the majority of DDM being retained inside the dialysis tubing with CymA. The dialysed CymA was loaded on to a Q-Sepharose anion-exchange column pre-equilibrated with 20 mM NaHepes (pH 7) containing 0.05 % DDM. The column was washed with 10 column vol. of 20 mM NaHepes (pH 7) containing 0.05 % DDM and then 20 mM NaHepes (pH 7) containing 0.05 % DDM and 50 mM NaCl. CymA samples with the lowest quinone content as evidenced by the ratio of

electronic absorbance at 270 nm (quinone) compared with 407 nm (haem) eluted with 20 mM NaHepes containing 0.05 % DDM and 130 mM NaCl. These samples were then concentrated and subjected to size-exclusion chromatography on a HiLOAD S200 Superdex column (GE Healthcare) in 25 mM NaHepes containing 0.05 % DDM yielding CymA with a typical absorbance ratio, A_{407nm}/A_{275nm}, of 4.

Biochemical analyses

All of the SDS/PAGE analyses were performed using the Laemmli discontinuous buffer method with 15 % polyacrylamide separating gels. Gels were developed for protein detection by Coomassie Brilliant Blue staining and for haem detection using the haem-linked peroxidase activity [26]. Immunoblotting for the V5 tag used the alkaline phosphatase method for detection of the relevant antibodies. MALDI–TOF-MS (matrix-assisted laser-desorption ionization–time-of-flight MS) analysis was performed at the Institute of Food Research and John Innes Centre Proteomics Facility (Norwich, U.K.). The predicted masses of the tryptic digests were determined using the ExPASy PeptideMass online software (Swiss Institute of Bioinformatics). N-terminal sequencing was performed at the Protein and Nucleic Acid Chemistry Facility at Cambridge University (Cambridge, U.K.). The haem content was determined using the pyridine haemochrome method [36] giving a value for the moral absorption coefficient at 407 nm, ε_{407nm}, of 380 ± 38 $mM^{-1} \cdot cm^{-1}$ for the oxidized protein assuming four haems per CymA monomer. Electronic absorption spectra were recorded on a JASCO V650 spectrophotometer. EPR spectra were recorded using a spectrometer comprising an ER-200D electromagnet and microwave bridge interfaced to an EMX control system (Brüker, Spectrospin) and fitted with a liquid helium flow cryostat (ESR-9, Oxford Instruments) and a dual-mode X-band cavity (Brüker, type ER4116DM).

To assess the Q content of CymA fractions eluted from the HiLOAD S200 Superdex column they were subject to solvent extraction (twice) with aqueous methanol/acetone (50/50 v/v) and petroleum ether (60/40 v/v) using the method of Myers and Myers [15]. Briefly, this involved stirring 0.5 ml of protein sample, typically 0.1–0.5 μM CymA, with 3 ml of acetone/methanol for 30 min followed by the addition of 1 ml of petroleum ether and stirring for 1 min. After the aqueous and organic layers had separated the Q-containing petroleum ether layer was pipetted off and evaporated under nitrogen gas. The Q extract was resuspended in 100 μl of ethanol/methanol (50/50 v/v) and resolved by HPLC analysis with a reverse-phase C18 (5 μm) column (dimensions 150 mm×4.6 mm; Phenomenex) with ethanol/methanol (50/50 v/v) as the mobile phase. The eluate was monitored by electronic absorbance at 248 nm, 270 nm and 290 nm to distinguish menaquinones (peak maxima at 248 nm and 270 nm) from ubiquinones (290 nm peak maximum). Comparison with the elution profile of standard solutions of menaquinone-7 ($\varepsilon_{248nm} = 18.9$ $mM^{-1} \cdot cm^{-1}$; Wako Chemicals) identified this as the major Q in the sample (retention time 30 min, flow rate 0.3 $ml \cdot min^{-1}$).

HQNO-binding assays

Fluorescence-quench titrations were performed to determine the affinity of CymA for HQNO [37]. Experiments were carried out with CymA solutions of the desired concentration in 100 mM Mops, 5 mM EDTA and 0.05 % DDM (pH 7) at room temperature (20°C). HQNO (>99 % purity; Enzo Life Sciences) was added as aliquots from a stock solution of 100, 250 or 500 μM in ethanol/water (30/70 v/v). Fluorescence intensities were measured using an excitation wavelength of 341 nm and an emission wavelength of 479 nm using a Varian Cary Eclipse Fluorescence Spectrophotometer. Variation of fluorescence intensity (F_{obs}) with HQNO concentration was fitted to eqn 1 that describes reversible binding of a single HQNO molecule to a single site on CymA [37]:

$$F_{obs} = f_{free}\left[HQNO_{total}\right] + (f_{bound} - f_{free}) \times (Q - \sqrt{Q^2 - \left[CymA_{total}\right]\left[HQNO_{total}\right]}) \quad (1)$$

with:

$$Q = \frac{1}{2}(\left[HQNO_{total}\right] + K_d + [CymA_{total}]) \quad (2)$$

and:

$$[HQNO_{total}] = [HQNO_{bound}] + [HQNO_{free}] \quad (3)$$

where f_{bound} and f_{free} are the specific fluorescence of bound and free HQNO respectively, K_d is the dissociation constant for binding of HQNO, and CymA and the subscripts 'total', 'bound' and 'free' refer to total, bound and free forms of the molecule respectively.

Potentiometric titration

All experiments were performed using spectroelectrochemical cells employing a three-electrode configuration that allowed a defined voltage to be applied to the sample. Cyclic voltammetry and amperometry were performed with an Autolab PGSTAT12 potentiostat under the control of GPES software. Studies of CymA adsorbed on to mesoporous nanocrystalline SnO_2 electrodes were performed using the spectroelectrochemical cells described previously [38]. Spectropotentiometric titration of CymA solutions monitored by MCD (magnetic circular dichroism) were typically performed with 10 μM CymA in 20 mM NaHepes and 100 mM NaCl (pH 7) containing a mediator cocktail lacking Qs and their analogues that comprised 40 μM each of: potassium ferricyanide ($E_m \sim +0.42$ V), ferrocene acetic acid ($E_m \sim +0.36$ V), diaminodurene ($E_m \sim +0.25$ V), dichlorophenol-indophenol ($E_m \sim +0.22$ V), phenazine methosulfate ($E_m \sim +0.08$ V), phenazine ethosulfate ($E_m \sim +0.05$ V), Methylene Blue ($E_m \sim +0.01$ V), Nile Blue ($E_m \sim -0.12$ V), phenosafranine ($E_m \sim -0.23$ V), Neutral Red ($E_m \sim -0.32$ V), Benzyl Viologen ($E_m \sim -0.35$ V), Sulfonyl Viologen ($E_m \sim -0.39$ V) and Methyl Viologen ($E_m \sim -0.44$ V). Equilibration of the sample at desired potentials was achieved using a gold-mini-grid working electrode as described previously [38]. Room temperature MCD spectra were recorded in a magnetic field of 8 Tesla using a circular dichrograph, JASCO J-710, together with an Oxford Instruments split-coil superconducting magnet fitted with a 50 mm ambient temperature bore. All potentials are quoted compared with the SHE at pH 7.0.

Assays of QH_2 oxidation coupled with CymA reduction

All of the sample manipulations were performed under strict anaerobic conditions in an N_2-filled glove-box (atmospheric O_2<4 p.p.m.). Solutions containing the desired concentrations of NADH, menadione (2-methyl-1,4-naphthoquinone), CymA, Fcc_3 and fumarate in 20 mM NaHepes and 0.5 mM EDTA (pH 7)

were stirred for 30 min in the glove-box prior to placing them in a 1-cm path-length cuvette that was subsequently sealed against the external atmosphere. The assay was initiated by the addition of *Clostridium kluyveri* diaphorase (Sigma–Aldrich) and the oxidation of NADH monitored by the decrease in absorbance at 340 nm. Experiments to investigate the extent to which the CymA haems were reduced by QH_2 were performed using a similar protocol, but excluding Fcc_3 and fumarate. Electronic absorbance spectra were measured between 300 nm and 700 nm. Concentrations of menadione were determined using $\varepsilon_{248nm} = 18.9\ mM^{-1}\cdot cm^{-1}$. When concentrated solutions of menadiol were required these were produced by electrodic reduction of menadione in an electrochemical cell employing a three-electrode configuration and graphite working electrode.

RESULTS

Expression, purification and catalytic activity of CymA

The pBAD-TOPO expression vector that features an L-arabinose inducible promoter and fuses a V5-epitope and His_6 tag to the C-terminus of the protein has been shown previously to produce *Shewanella* sp. strain ANA-3 CymA in the parent strain and to complement a *cymA* deletion strain [39]. Consequently this vector was employed to express *S. oneidensis* MR-1 *cymA* in the parent strain. Purification of recombinant CymA from *S. oneidensis* MR-1 membranes was achieved through a combination of anion-exchange and gel-filtration chromatographies since the protein did not bind avidly to metal-ion affinity columns. The resulting protein was judged to be greater than 90 % pure from a combination of SDS/PAGE, MS, N-terminal sequencing and electronic-absorption spectroscopy. Native CymA of comparable purity was obtained from *S. oneidensis* MR-1 membranes by minor modification of a previously described protocol [26]. The electronic absorbance spectra, redox properties and catalytic activity of the recombinant and native proteins were indistinguishable as described below. However, the significantly higher yields of recombinant than native CymA allowed EPR and MCD spectroscopies to be employed for greater structural insight. Consequently the data presented below were collected from recombinant protein that for simplicity is termed CymA in the text below.

The QH_2 dehydrogenase activity of purified CymA was investigated through a coupled assay that measured the loss of absorbance at 340 nm due to the NADH-dependent reduction of fumarate to succinate. The assay employed the sequential activities of diaphorase, as an NADH–Q oxidoreductase, CymA to oxidize QH_2, and then the soluble fumarate reductase Fcc_3 from *S. oneidensis* MR-1 to pass electrons from CymA to fumarate. A rate of 0.6 ± 0.1 NADH oxidized min^{-1}. $CymA^{-1}$ was measured on initiating the assay by the addition of diaphorase (1.5 μM) to a solution containing 50 μM NADH, 1.2 μM menadione, 0.2 μM CymA, 1 μM Fcc_3 and 1 mM fumarate at pH 7. The calculated rate value has been corrected for the background rate of NADH auto-oxidation, 0.05 ± 0.01 μM NADH oxidized$\cdot$ min^{-1}, determined in control assays which contained menadione, Fcc_3 and fumarate, but no CymA.

Primary structure, electrophoretic profile and oligomeric state

The theoretical peptide mass of recombinant CymA is 24.3 kDa and for the holoprotein with four *c*-type haems inserted is 26.8 kDa. SDS/PAGE analysis of purified CymA visualized by Coomassie Brilliant Blue stain revealed a major band at approximately 24 kDa corresponding to the predicted mass of the monomer (Figure 1). This was confirmed as CymA through N-terminal sequencing that identified the predicted residues (MNWRA) and positive responses in immunoblots for the V5 epitope (Figure 1). Tryptic digest followed by MALDI–TOF-MS identified three fragments with the predicted peptide masses for CymA digestion products lacking covalently bound haem (Supplementary Table S1 at http://www.BiochemJ.org/bj/444/bj4440465add.htm).

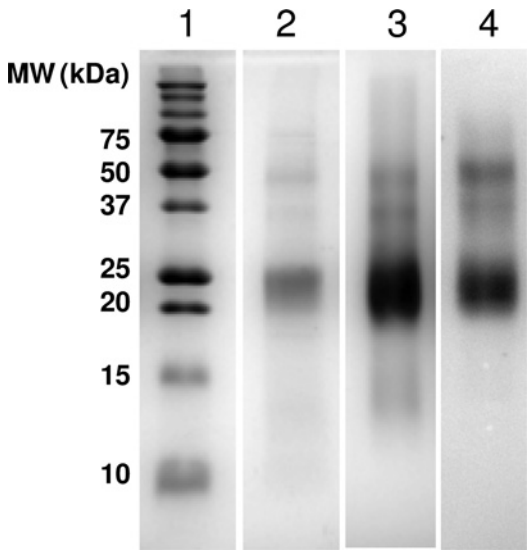

Figure 1 SDS/PAGE of CymA

Protein visualized by Coomassie Brilliant Blue stain (lane 2), haem stain (lane 3) and immunoblot against the anti-V5 epitope (lane 4). Molecular mass markers are shown for comparison (lane 1). Protein was loaded at 2 μg for Coomassie Brilliant Blue staining, 0.5 μg for haem staining and 0.8 μg for the immunoblot.

In addition to the band at approximately 24 kDa identified by SDS/PAGE, minor bands were detected at approximately 40 and 50 kDa. All three of the bands stained positively for the presence of *c*-type haem using haem-linked peroxidase staining (Figure 1). The 40 and 50 kDa bands were confirmed as CymA by positive staining in an immunoblot for the V5 epitope (Figure 1), and the fragmentation patterns following MS of tryptic digests. The higher-molecular-mass bands could arise from partially unfolded protein or oligomeric forms. Consequently dynamic light scattering and gel filtration were used to provide direct insight into the oligomeric state of native CymA in solutions containing approximately 0.05 % DDM as used throughout the present study. The mass of a DDM micelle is approximately 50 kDa and this would rise to approximately 75 kDa on inclusion of a CymA monomer and approximately 100 kDa on inclusion of a CymA dimer. Dynamic light scattering of CymA (80 μM) reported a hydrodynamic radius of 8 nm, corresponding to a mass of approximately 95 kDa, with a polydispersity of 35 % that is indicative of a sample of homogeneous size, shape and mass distribution. In gel-filtration chromatography, the DDM-solubilized CymA eluted as a single peak with an apparent molecular mass of approximately 130 kDa. Both results support the presence of a CymA dimer within the DDM micelle.

Spectral properties

The electronic absorbance spectrum of oxidized CymA in the visible region is dominated by features typical of low-spin ($S = {}^1/_2$) ferric *c*-haems, namely, a Soret band with a maximum

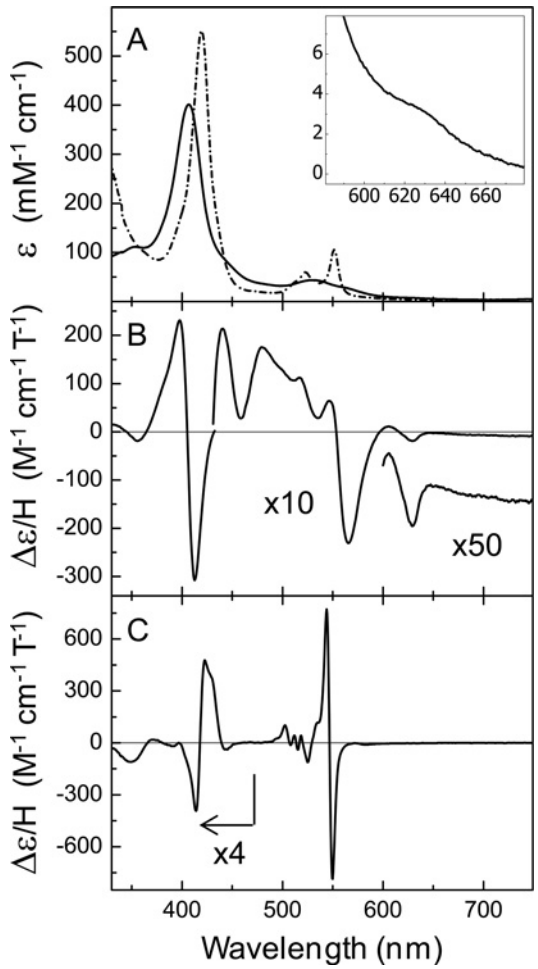

Figure 2 Spectroscopic characterization of CymA

(**A**) Electronic absorbance spectra for CymA oxidized (solid line) and fully reduced by dithionite (broken line). Inset, an expanded view of the spectrum of oxidized CymA between 580 and 700 nm. MCD spectra measured at ambient temperature for oxidized (**B**) and fully dithionite reduced (**C**) CymA. In each case the buffer was 20 mM Hepes at pH 7.0 containing approximately 0.05 % DDM. For MCD of reduced CymA the enzyme was 10 μM and for oxidized enzyme it was 20 μM for the Soret region and 80 μM for 450–800 nm.

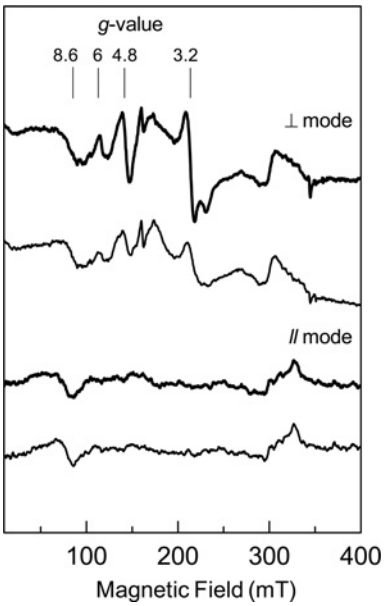

Figure 3 X-band EPR spectra for CymA with and without HQNO bound

Fully oxidized CymA (80 μM) in the absence (thick lines) and presence (thin lines) of HQNO (270 μM) in 20 mM Hepes and 0.05 % DDM at pH 7.0. Spectra were recorded at 10 K with 100 mW microwave power and modulation amplitude of 10 Gauss in the perpendicular mode (microwave frequency 9.7 GHz) and parallel mode (9.4 GHz) as indicated.

at 407 nm and a broad absorbance between 500 and 600 nm corresponding to the α/β bands (Figure 2A). However, closer inspection of the higher-wavelength region of the spectrum reveals a broad feature with a peak at 630 nm. Such features typically arise from LMCT (ligand-to-metal charge-transfer) bands associated with high-spin ($S = {}^5/_2$) ferric haems. They are more clearly visualized by MCD where their wavelength is diagnostic of the chemical nature of the axial haem ligands [40]. MCD of CymA presents a clear bisignate feature with a trough at 628 nm that is indicative of a histidine- or lysine-co-ordinated haem having water as the second axial ligand (Figure 2B). This feature has an intensity of 3 $M^{-1}\cdot cm^{-1}\cdot T^{-1}$ that compares with typical intensities of 1–4 $M^{-1}\cdot cm^{-1}\cdot T^{-1}$ per high-spin ferric haem and it lies in a spectral region that is free from contributions from low-spin haem [40]. At wavelengths below 600 nm the MCD of CymA is dominated by features characteristic of low-spin ferric *c*-haem with the most prominent of these in the Soret region having a peak-to-trough intensity of 540 $M^{-1}\cdot cm^{-1}\cdot T^{-1}$. For low-spin ferric haems the peak-to-trough intensity of the prominent Soret feature is typically 150 ± 10 $M^{-1}\cdot cm^{-1}\cdot T^{-1}$ compared with a maximal intensity of 20 $M^{-1}\cdot cm^{-1}\cdot T^{-1}$ for high-spin ferric haem [41]. Given these reference intensities and a molar absorption coefficient at 407 nm of 380 ± 38 $mM^{-1}\cdot cm^{-1}$ for oxidized CymA, as described in the Experimental section, the MCD spectrum is consistent with the presence of one high-spin and three low-spin haems as the nearest integer values.

X-band EPR spectra of oxidized CymA in the perpendicular mode resolved prominent features with *g* values of ~ 8.6, 4.8 and 3.2 (Figure 3). The features at $g \sim 8.6$ and ~3.2, with the former retained in parallel mode, are typical of an integer spin species arising from a coupled high-/low-spin haem pair as seen in other multihaem cytochromes including the cytochrome c_{m552} ubiquinone reductase purified from *Nitrosomonas europaea* in the absence of a periplasmic redox partner [27,42]. The signals between $g \sim 3$ and 5 may arise from exchange-coupled low-spin haems. The relatively sharp resonance with zero crossing at $g = 4.8$ seen in the perpendicular mode EPR of CymA is unusual. However, it is also displayed by the NrfHA complexes of *Wolinella succinogenes, Desulfovibrio desulfuricans* and *D. vulgaris* where it was proposed to arise from spin-coupled haems in NrfH since it is absent from spectra of NrfA [43]. Significantly, there is no evidence for features attributable to the rhombic trios or large g_{max} signals that would typically arise from uncoupled low-spin ferric haem. The feature at $g \sim 6$ that arises from uncoupled high-spin ferric haem represents only a very small fraction of the protein concentration. When all features of the EPR spectrum are taken together it is apparent that the spins of all of the haems in oxidized CymA are electronically coupled and this conclusion is supported by the low intensity of the EPR features relative to the CymA concentration. Importantly the overall description of CymA as containing both low- and high-spin ferric haems is consistent with that deduced from optical spectroscopies.

Dithionite reduction of CymA results in the appearance of maxima at 551.5, 520 and 420 nm in the electronic absorption spectrum that are typical for the α-, β- and Soret-features arising from reduced low-spin ferrous *c*-haem (Figure 2A). The MCD

of dithionite-reduced CymA confirms the complete reduction of the haems since there is no indication of features typical of either low- or high-spin ferric haems (Figure 2C). Instead the spectrum is dominated by a sharp bisignate feature centred on 548 nm with a peak-to-trough intensity of 1400 $M^{-1}\cdot cm^{-1}\cdot T^{-1}$ arising from low-spin ferrous haem. The bisignate feature in the Soret region with a trough at approximately 443 nm and peak at approximately 430 nm of 90 $M^{-1}\cdot cm^{-1}\cdot T^{-1}$ is indicative of the presence of high-spin ferrous haem. The intensity at 430 nm, arising from high-spin ferrous haems, is typically of the order of 100 $M^{-1}\cdot cm^{-1}\cdot T^{-1}$, whereas the peak-to-trough intensity of the bisignate feature centred on 552 nm arising from low-spin ferrous haem is typically of the order of 400 $M^{-1}\cdot cm^{-1}\cdot T^{-1}$ [38,44]. The MCD intensity from the ferrous haems is, like that from the ferric haems, consistent with nearest integer values of one high-spin and three low-spin centres given the uncertainty in the molar absorption coefficient of CymA noted above.

HQNO binding

The QH_2-binding affinity of oxidized CymA was measured using the menaquinol analogue HQNO since the fluorescence of the latter is quenched when it binds to a protein in the vicinity of a haem co-factor (see [39] and references therein). In the absence of CymA the intensity of fluorescence arising from HQNO increases in direct proportion to its concentration (Figure 4A). When HQNO is titrated into a solution of CymA this fluorescence is quenched until the binding sites become saturated (Figure 4A). Following this point the fluorescence increases in a linear manner reflecting the presence of free HQNO. The slope of the linear region of these plots decreases as the concentration of CymA increases. This is behaviour that has been noted in other studies, e.g. [37,39], and it results from non-specific quenching of the HQNO fluorescence that prevents the affinity of HQNO for a membrane protein being defined simply by titration of the protein into a solution of fixed HQNO concentration. Consequently, the data of Figure 4(A) were fitted to eqns (1)–(3) that describe reversible 1:1 binding of HQNO to CymA with $K_d = 0.5 \pm 0.3$ μM.

When a 20-fold excess of HQNO was added to 20 μM CymA such that essentially all of the enzyme had bound HQNO there was little change in the electronic absorbance spectrum through the Soret and α/β regions (Figure 4B). In contrast, a clear spectral change was noted between 550 and 700 nm that is most readily appreciated in the difference spectrum where the high-spin ferric haem charge-transfer band shifts to longer wavelength and narrows on HQNO binding (Figure 4B, inset). Thus HQNO binding perturbs the environment of the high-spin haem without changing the net spin states of the haems. This conclusion was confirmed by MCD where the binding of HQNO results in negligible change between 350 and 600 nm where the spectrum is dominated by contributions from low-spin ferric haem (Supplementary Figure S1, upper panel at http://www.BiochemJ.org/bj/444/bj4440465add.htm). In contrast, the charge-transfer band at 628 nm broadens reflecting an altered environment of the high-spin ferric haem. In agreement with these observations, the EPR of CymA with bound HQNO retains the feature at $g \sim 8.6$ arising from an exchange-coupled high-spin/low-spin haem pair and shows only subtle changes of intensity for some of the other spectral features (Figure 3). The MCD of dithionite-reduced CymA with HQNO bound was indistinguishable from that of the reduced enzyme in the absence of HQNO (Supplementary Figure S1, lower panel). Thus one high-spin and three low-spin haems are present in reduced HQNO-bound CymA as for the oxidized enzyme.

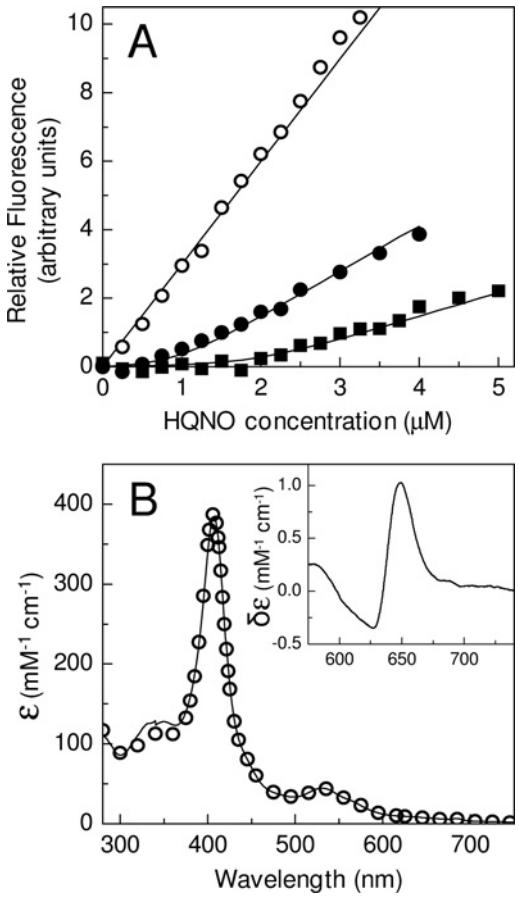

Figure 4 Optically monitored HQNO binding to CymA

(**A**) Representative HQNO fluorescence in the presence of 0 (○), 1 (●) and 3 (■) μM CymA in 100 mM Mops, 5 mM EDTA and 0.05 % DDM at pH 7.0. (**B**) Representative electronic absorbance spectra for 20 μM CymA before (○) and after (solid line) the addition of 400 μM HQNO in 20 mM Hepes and 0.05 % DDM at pH 7.0. Inset: difference in the absorbance of HQNO-bound and HQNO-free CymA.

Spectropotentiometry

MCD most clearly resolves signals from both the low- and high-spin states of the ferric and ferrous haems in CymA. Consequently, potentiometric titration monitored by MCD spectroscopy was employed in initial experiments to resolve the redox behaviour of CymA in the presence and absence of bound HQNO (Figures 5A and 5B). In both cases spectra typical of the fully oxidized enzyme were recorded at potentials above 0 mV. Samples poised below − 40 mV displayed the sharp bisignate feature centred on 548 nm that is characteristic of low-spin ferrous haem. In contrast, the positive feature at 430 nm that is diagnostic of high-spin ferrous haem was detected only below − 150 mV. An MCD-compatible optically transparent thin-layer electrochemical cell was used to facilitate the collection of these data [45]. Nevertheless, full reduction of CymA in a practical timescale was prevented by the long equilibration times (typically >30 min) resulting from slow diffusion in DDM that were compounded if large changes in potential were applied to the sample. Consequently, the redox properties of the low-spin haems were quantified by normalizing the peak-to-trough MCD intensity of the feature at 548 nm to that displayed by fully dithionite-reduced CymA. A similar strategy was adopted to quantify reduction of the high-spin haem after accounting for changes in intensity at 430 nm due to the loss of signal from the low-spin ferric haems (Figure 5A). Plotting these

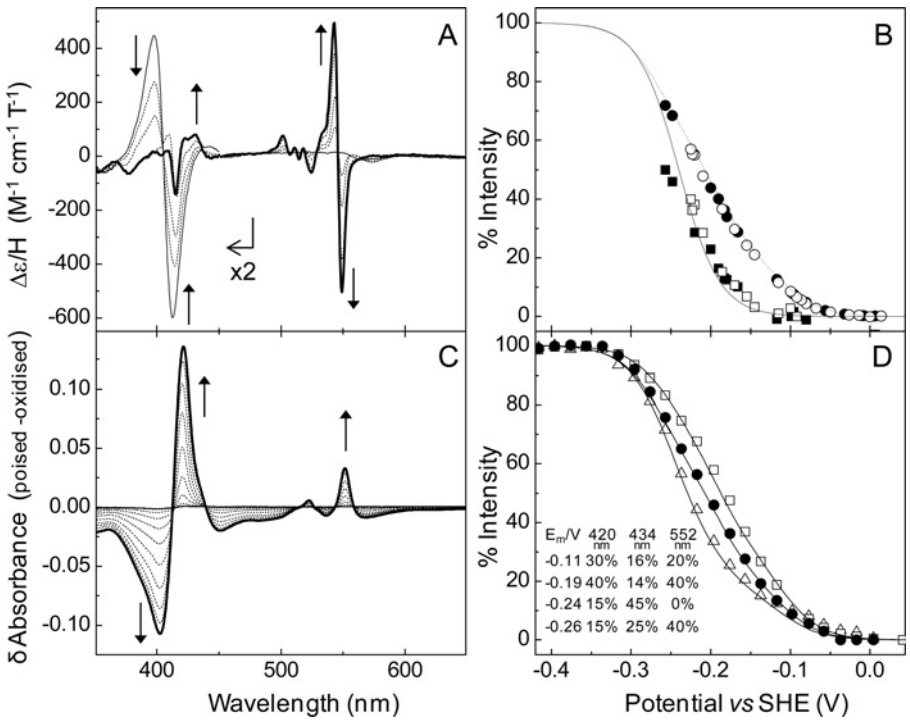

Figure 5 Spectropotentiometric titration of CymA

(**A**) MCD monitored potentiometry of CymA (10 μM) in the presence of HQNO (200 μM) in 20 mM Hepes and 100 mM NaCl (pH 7.0) and approximately 0.05 % DDM. Spectra were recorded for the sample equilibrated at 0 V (thin solid line), -0.12 V, -0.17 V, -0.22 V (broken lines) and -0.26 V (heavy solid line). Arrows indicate the direction of spectral change on reduction. (**B**) The potential dependence of MCD intensity at 550 nm (circles) and 430 nm (squares) for CymA in the absence (open symbols) and presence (closed symbols) of HQNO. The intensity at each wavelength is plotted as a percentage of that displayed by fully reduced CymA (Figure 2C). The solid line describes Nernstian behaviour for a single $n=1$ centre with $E_m = -0.24$ V. The broken line describes the sum of three Nernstian responses for $n=1$ centres contributing equally to the intensity change and having E_m values of -0.11 V, -0.19 V and -0.265 V. (**C**) Potentiometric titration of CymA adsorbed on SnO_2 electrodes and equilibrated at potentials between $+0.04$ V and -0.4 V in 20 mM Hepes and 100 mM NaCl (pH 7.0). Data are plotted as the difference spectra, poised-minus-oxidized, arrows indicate the direction of spectral change on reduction. (**D**) Potential dependence of absorbance change at 420 nm (□), 434 nm (△) and 552 nm (●). Lines show the sum of Nernstian behaviours for $n=1$ redox centres with $E_m = -0.11$ V, -0.19 V, -0.24 V and -0.26 V and the relative contributions indicated.

normalized signal intensities as a function of sample potential provided no evidence for a change in the redox properties of CymA on binding HQNO (Figure 5B).

CymA was adsorbed as an electrochemically active film on optically transparent mesoporous nanocrystalline SnO_2 electrodes in order to gain an independent assessment of its redox chemistry over a wider potential window than accessible to the MCD-compatible cell (Figures 5C and 5D). Equilibration at any given potential was achieved within 5 min and electronic absorption spectroscopy of the film poised at potentials from $+40$ to -400 mV revealed the spectral changes anticipated for the transformation of fully oxidized to fully reduced CymA. These changes are readily visualized in difference spectra where the spectrum of fully oxidized CymA (poised at $+40$ mV) has been subtracted from those of the sample poised at other potentials and where isosbestic points occur at 412, 439, 543 and 559 nm (Figure 5C). The absorbance at 552 nm arises solely from low-spin haem. There was no hysteresis in the potential dependence of this absorbance over multiple cycles of reduction and oxidation. Consequently it can be concluded that redox transformation of the three low-spin ferric haems is fully reversible.

The spectral changes in the Soret region contain information relating to the redox transformation of the high-spin haem in CymA. However, this information is superimposed on that from spectral changes that describe redox transformation of the low-spin haems. The spectral changes from the high-spin haems extend to slightly longer wavelengths (>approximately 420 nm) than for their low-spin counterparts such that in favourable cases it is possible to clearly resolve redox transformation of low- and high-spin haems [38]; however, this is not the case for CymA. Consequently, a global analysis of the data at 552, 434 and 420 nm was performed to resolve E_m values for the one high-spin and three low-spin haems (Figure 5D). It was assumed that each haem behaves as an isolated single electron ($n=1$) centre described by the Nernst equation. The following constraints were also applied: (i) the absorbance changes at 552 nm must arise only from three low-spin haems; and (ii) the changes of absorbance at 420 and 434 nm must arise from one high-spin and three low-spin haems with the former making a more significant contribution to the magnitude of the spectral change at 434 than 420 nm. This analysis resolved E_m values of -110, -190 and -265 mV for the low-spin haem and -240 mV for the high-spin haem, where all values are ± 30 mV (Figure 5D). These E_m values provided a good description of the MCD monitored potentiometry where spectral features arising purely from both low- and high-spin haems are more readily revealed, as described above (Figure 5B).

CymA reduction by QH_2

The low solubility of menaquinols in aqueous solution makes it difficult to design an experiment to confidently assess their ability to reduce DDM-solubilized CymA. Consequently, the reduction of CymA by QH_2 was probed using menadiol, a water-soluble analogue of menaquinol. Menadione and menaquinone have comparable reduction potentials. By itself excess menadiol (×30)

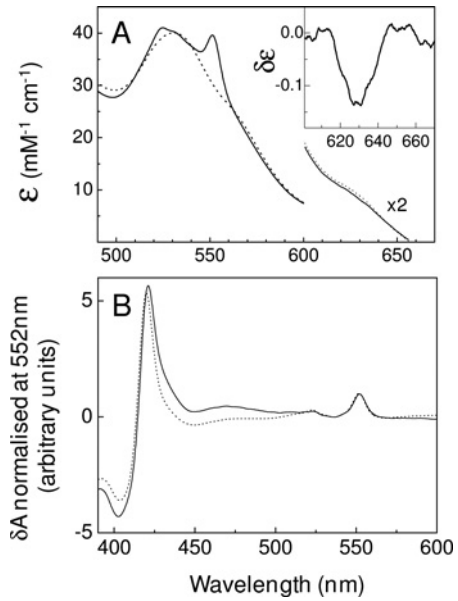

Figure 6 Reduction of CymA by menadiol

(**A**) Representative electronic absorbance spectra of 4.6 μM CymA equilibrated with 7 μM menadione and 240 μM NADH (broken line) and 15 min after the addition of diaphorase (solid line). Inset, the difference spectrum, reduced-minus-oxidized, for the charge-transfer band at 628 nm. (**B**) Representative reduced-minus-oxidized difference spectra for 1 μM CymA (solid line) and 1 μM CymA with 1 μM Fcc_3 (broken line) for the reduction by 100 μM NADH, diaphorase and 10 μM menadione. In each case the buffer was 20 mM Hepes and 0.5 mM EDTA (pH 7.0) containing 0.05 % DDM.

did not produce any evidence for reduction of CymA. However, CymA reduction was observed when NADH and diaphorase were included in order to provide a greater driving force for the reduction and couple NADH oxidation to menadione reduction (Figure 6A, solid line). Subsequent addition of dithionite to completely reduce CymA allowed the extent of reduction to be quantified. A 20 % reduction of CymA by NADH was indicated by both the absorbance increase at 552 nm and the absorbance decrease at 630 nm corresponding to reduction of low- and high-spin haems respectively. Reduced-minus-oxidized difference spectra confirmed the reduction of low-spin haem through the positive features at 420, 523 and 552 nm and reduction of the high-spin haem through the 430 nm shoulder on the Soret feature (Figure 6B, solid line). The extent of CymA reduction is not changed significantly when the concentrations of NADH and menadione are raised to 2 and 0.5 mM respectively (results not shown).

The extent of CymA reduction by NADH, diaphorase and menadione was also investigated in the presence of the redox partner Fcc_3 fumarate reductase that contains four low-spin *c*-haems. The absorbance increase at 552 nm was used to assess the extent of low-spin haem reduction and the redox difference spectrum to assess reduction of high-spin haem. With the concentration of Fcc_3 equal to that of CymA, the increase in absorbance at 552 nm was 20 % of that achieved for full dithionite reduction of all haems in the sample. The redox difference spectrum showed evidence of a positive shoulder on the Soret feature at 430 nm confirming reduction of the high-spin haem in CymA against reduction of a relatively larger proportion of low-spin haems owing to the presence of Fcc_3 (Figure 6B, broken line). There was no reduction in Fcc_3 in the absence of CymA.

DISCUSSION

The proposed dimer formed by CymA is likely to be stabilized by interprotein interactions mediated by the periplasmic globular domain in addition to the GxxxG motif of the membrane-spanning helix as described for *D. vulgaris* NrfH [16]. However, *S. oneidensis* MR-1 CymA contains 28 more amino acids than *D. vulgaris* NrfH including 17 more residues between the CxxCH motifs that bind haems III and IV. This makes it difficult to accurately predict the complete structure of CymA from an alignment-based homology model [27,46]. Certainly the MCD of *S. oneidensis* MR-1 CymA provides no evidence for a methionine-ligated penta-co-ordinate haem as found in NrfH. A similar conclusion was drawn from MCD of *S. frigidimarina* CymA by Richardson and colleagues [26]. In that study, LMCT bands resolved by MCD at near-infra-red wavelengths identified His/His-ligated low-spin ferric haems in the oxidized enzyme. The reduced enzyme displayed positive MCD intensity at 430 nm alongside a sharp bisignate feature at 552 nm indicative of high- and low-spin ferrous haem respectively. This led the authors to propose that *S. frigidimarina* CymA contained four His/His-ligated ferric haems and that one histidine residue dissociated on reduction of the enzyme. However, and as noted above, the spectral properties of high-spin ferric haem make such centres difficult to detect when their low-spin counterparts are present. Close inspection of the MCD of 100 μM oxidized *S. frigidimarina* CymA [26] resolves a broad bisignate feature between 610 and 660 nm that is indicative of high-spin ferric haem. Consequently, we propose that the CymA enzymes of *S. frigidimarina* and *S. oneidensis* MR-1 have the same haem ligation in all oxidation states, namely, three haems with His/His-ligation and one high-spin haem ligated by a nitrogenous amino acid and with either water, hydroxide or a vacancy at the second axial site.

DDM-solubilized oxidized CymA displays an affinity for HQNO ($K_d \sim 0.5$ μM) that is comparable with that reported for CymA from *Shewanella* sp. strain ANA-3 in cytoplasmic membranes [39]. Binding HQNO does not alter the ratio of high- to low-spin haems. However, the LMCT band from the high-spin ferric haem shifts to a longer wavelength on HQNO binding that may indicate formation of penta-co-ordinate haem through loss of the water ligand. HQNO binds adjacent to haem I in NrfH [17] so we consider the high-spin haem of CymA to be haem I. Sequence alignments together with results of site-specific mutagenesis of NapC/NirT family members and the structure of NrfH then allow us to propose amino acid ligands to the CymA haems as follows. Either His^{50}, of the first CxxCH haem-binding motif, or His^{53} will form the nitrogenous ligand to haem I since in *D. vulgaris* NrfH it is Met^{49} rather than His^{47} of the CxxCH binding motif that ligates haem I. The low-spin haems II, III and IV would then be ligated by His^{79}/His^{182}, His^{140}/His^{64} and His^{177}/His^{159} respectively, where the first histidine of each pair is that from the CxxCH motif [47,48]. A unified description of QH_2 oxidation by haem with a single axial ligand provided by an amino acid may then be appropriate for NapC/NirT homologues.

At pH 7, the midpoint potentials of the CymA haems of approximately -110, -190, -240 and -265 mV were not altered detectably by HQNO binding. This agrees with the results of voltammetric studies of CymA attached to modified gold electrodes [49] and it indicates that HQNO has equal affinity for all oxidation states of CymA. If this situation extends to the descriptions of CymA with Q and QH_2 bound there is a thermodynamic disposition for intraprotein electron transfer from haem I ($E_m = -240$ mV) to the low-spin haems following reduction by QH_2 that may serve to minimize the life-time of semi-quinone radicals during QH_2 oxidation. That

CymA is not reduced to any significant extent by menadiol is consistent with the menadione–menadiol couple (E_m value of approximately −80 mV) having a higher midpoint potential than the CymA haems. Adding the NADH–Q oxidoreductase diaphorase together with a significant excess of NADH (E_m value of approximately −320 mV) to increase the reductive driving force leads to reduction of CymA. However, in several repeats of this experiment only 20–30 % of the sample was reduced. There was no indication of rapid interprotein electron transfer that would serve to equilibrate oxidation state across the entire population of CymA in the sample. This is in contrast with the complete reduction of the CymA sample achieved by the addition of excess dithionite or equilibration at −350 mV by direct, or mediated, electrodic reduction. It must be concluded that the population of CymA behaves heterogeneously when electrons are supplied by menadiol, an analogue of the natural menaquinol substrate, which is presumably oxidized at a specific site in the vicinity of haem I.

No evidence for heterogeneity in the spectral or redox properties of CymA was found when the protein was manipulated electrodically or in HQNO-binding studies. The heterogeneity of the CymA sample with respect to menadiol reduction does though imply that the assays of QH_2 oxidation coupled to fumarate reduction underestimate by 4-fold the rates that may be supported by CymA. Sample heterogeneity is not uncommon in studies of membrane proteins where their separation from lipids and Qs can be extremely difficult to monitor and achieve completely. For CymA it suggests that a co-factor other than haem is required for QH_2 oxidation. Elsewhere, we report a voltammetric characterization of CymA that shows a requirement for menaquinol-7 in order for the enzyme to be catalytically active towards menadione [49]. It is possible that in the experiments reported in that paper only a fraction of the purified CymA has a menaquinone-7 bound and that it is this fraction that is amenable to reduction by menadiol.

Considering these observations in the context of the anaerobic respiratory flexibility displayed by *S. oneidensis* MR-1 several points can be made. We cannot exclude that significantly different E_m values or QH_2-binding properties are displayed by CymA in cytoplasmic membranes when compared with DDM micelles; however, this seems unlikely. The majority of the haem-containing globular domain is located in the periplasm and the HQNO-binding properties of DDM-solubilized CymA compare favourably with those displayed by the enzyme in cytoplasmic membranes [39]. Consequently, the redox poise of the menaquinol pool by itself is unlikely to produce significant reduction of CymA. The formal potentials of the $CO_2/HCOO^-$ and H^+/H_2 couples in the cell will, like that of the NAD^+/NADH couple, lie in the vicinity of −300 to −400 mV. Depending on growth conditions, electrons entering the menaquinol pool via the activity of primary dehydrogenases such as the proton-pumping NADH dehydrogenase or electrogenic formate dehydrogenase and hydrogenase should then provide sufficient driving force to reduce CymA via the menaquinol pool. CymA is not in itself proton-motive, but instead contributes to respiratory energy conversation by recycling the menaquinol pool. Electron transfer from menaquinol to the terminal electron acceptors mediated by the activity of CymA will also be favoured by the thermodynamic bias for that electron transfer, for example the fumarate/succinate couple has a standard reduction potential of approximately −30 mV at pH 7. Thus the thermodynamically unfavourable reduction of CymA by menaquinol may be overcome in the cellular context by its integration with an electrical circuitry that can regulate this electron flux at the levels of both electron supply and demand.

In closing we note that the heterogeneity of the CymA sample towards menadiol reduction provided an opportunity to gain insight into the nature of the interaction of CymA and its redox partner Fcc_3. Transient interactions were expected to allow a single molecule of CymA to partner different reductases in support of a respiratory plasticity that allows utilization of a wide variety of electron acceptors [50]. However, catalytic reduction of Fcc_3 by CymA was not observed. The extent of reduction in samples containing equal quantities of CymA and Fcc_3 was within error of that produced in a parallel experiment lacking Fcc_3. The formation of a stable 1:1 complex of the two reduced proteins is suggested. In the cellular context it may be that CymA exists in excess of certain of its periplasmic redox partners such that multiple 'hard-wired' complexes support respiratory flexibility. Experiments are underway to explore the possibilities presented above.

AUTHOR CONTRIBUTION

Julea Butt developed the project, designed the experiments, analysed the data and wrote the paper; Sophie Marritt led the experimental programme, assisted by Jordon Bye and Thomas Lowe, and contributed to experimental design, data analysis and writing of the paper; Liang Shi, Jim Fredrickson and John Zachara prepared the MR-1 strain overexpressing *cymA*; Myles Cheesman facilitated MCD and EPR data collection and analysis; Duncan McMillan and David Richardson contributed to the experimental design and data analysis; Julea Butt, Lars Jeuken, David Richardson, Jim Fredrickson and John Zachara secured funding for the project. All authors discussed the results and commented on the paper.

ACKNOWLEDGEMENTS

We thank Nick Cull for purification of the Fcc_3 fumarate reductase and Professor James Durrant and Dr Li Xiaoe (Imperial College London, London, U.K.) for the donation of mesoporous nanocrystalline tin dioxide electrodes.

FUNDING

This work was supported by the U.K. Biotechnology and Biological Sciences Research Council [grant number BB/G009228], the Subsurface Biogeochemical Research (SBR) program/Office of Biological and Environmental Research (BER), the U.S. Department of Energy (DOE), and the Pacific Northwest National Laboratory (PNNL) Scientific Focus Area (operated for the DOE by Battelle under contract DE-AC05-76RLO 1830). D.J.R. was supported by a Royal Society and Wolfson Foundation for a Merit Award Fellowship.

REFERENCES

1 Fredrickson, J. K., Romine, M. F., Beliaev, A. S., Auchtung, J. M., Driscoll, M. E., Gardner, T. S., Nealson, K. H., Osterman, A. L., Pinchuk, G., Reed, J. L. et al. (2008) Towards environmental systems biology of *Shewanella*. Nat. Rev. Microbiol. **6**, 592–603

2 Hartshorne, R. S., Reardon, C. L., Ross, D., Nuester, J., Clarke, T. A., Gates, A. J., Mills, P. C., Fredrickson, J. K., Zachara, J. M., Shi, L. et al. (2009) Characterization of an electron conduit between bacteria and the extracellular environment. Proc. Natl. Acad. Sci. U.S.A. **106**, 22169–22174

3 Bucking, C., Popp, F., Kerzenmacher, S. and Gescher, J. (2010) Involvement and specificity of *Shewanella oneidensis* outer membrane cytochromes in the reduction of soluble and solid-phase terminal electron acceptors. FEMS Microbiol. Lett. **306**, 144–151

4 Coursolle, D., Baron, D. B., Bond, D. R. and Gralnick, J. A. (2010) The Mtr respiratory pathway is essential for reducing flavins and electrodes in *Shewanella oneidensis*. J. Bacteriol. **192**, 467–474

5 Gralnick, J. A., Vali, H., Lies, D. P. and Newman, D. K. (2006) Extracellular respiration of dimethyl sulfoxide by *Shewanella oneidensis* strain MR-1. Proc. Natl. Acad. Sci. U.S.A. **103**, 4669–4674

6 Clarke, T. A., Edwards, M. J., Gates, A. J., Hall, A., White, G. F., Bradley, J., Reardon, C. L., Shi, L., Beliaev, A. S., Marshall, M. J. et al. (2011) Structure of a bacterial cell surface decaheme electron conduit. Proc. Natl. Acad. Sci. U.S.A. **108**, 9384–9389

7 Hau, H. H. and Gralnick, J. A. (2007) Ecology and biotechnology of the genus *Shewanella*. Annu. Rev. Microbiol. **61**, 237–258

8 Hunt, K. A., Flynn, J. M., Naranjo, B., Shikhare, I. D. and Gralnick, J. A. (2010) Substrate-level phosphorylation is the primary source of energy conservation during anaerobic respiration of *Shewanella oneidensis* strain MR-1. J. Bacteriol. **192**, 3345–3351

9 Simon, J., van Spanning, R. J. M. and Richardson, D. J. (2008) The organisation of proton motive and non-proton motive redox loops in prokaryotic respiratory systems. Biochim. Biophys. Acta **1777**, 1480–1490

10 Myers, C. R. and Nealson, K. H. (1990) Respiration-linked proton tranlocation coupled to anaerobic reduction of manganese(IV) and iron(III) in *Shewanella putrefaciens* MR-1. J. Bacteriol. **172**, 6232–6238

11 Myers, C. R. and Myers, J. M. (1997) Cloning and sequence of *cymA* a gene encoding a tetraheme cytochrome *c* required for reduction of iron(III), fumarate, and nitrate by *Shewanella putrefaciens* MR-1. J. Bacteriol. **179**, 1143–1152

12 Shi, L., Squier, T. C., Zachara, J. M. and Fredrickson, J. K. (2007) Respiration of metal (hydr)oxides by *Shewanella* and *Geobacter*: a key role for multihaem *c*-type cytochromes. Mol. Microbiol. **65**, 12–20

13 Schwalb, C., Chapman, S. K. and Reid, G. A. (2003) The tetraheme cytochrome CymA is required for anaerobic respiration with dimethyl sulfoxide and nitrite in *Shewanella oneidensis*. Biochemistry **42**, 9491–9497

14 Gao, H. C., Yang, Z. K., Barua, S., Reed, S. B., Romine, M. F., Nealson, K. H., Fredrickson, J. K., Tiedje, J. M. and Zhou, J. Z. (2009) Reduction of nitrate in *Shewanella oneidensis* depends on atypical NAP and NRF systems with NapB as a preferred electron transport protein from CymA to NapA. ISME J. **3**, 966–976

15 Myers, J. M. and Myers, C. R. (2000) Role of the tetraheme cytochrome CymA in anaerobic electron transport in cells of *Shewanella putrefaciens* MR-1 with normal levels of menaquinone. J. Bacteriol. **182**, 67–75

16 Rodrigues, M. L., Oliveira, T. F., Pereira, I. A. C. and Archer, M. (2006) X-ray structure of the membrane-bound cytochrome *c* quinol dehydrogenase NrfH reveals novel haem coordination. EMBO J. **25**, 5951–5960

17 Rodrigues, M. L., Scott, K. A., Sansom, M. S. P., Pereira, I. A. C. and Archer, M. (2008) Quinol oxidation by *c*-type cytochromes: structural characterization of the menaquinol binding site of NrfHA. J. Mol. Biol. **381**, 341–350

18 Berks, B. C., Richardson, D. J., Reilly, A., Willis, A. C. and Ferguson, S. J. (1995) The *napEDABC* gene-cluster encoding the periplasmic nitrate reductase system of *Thiosphaera pantotropha*. Biochem. J. **309**, 983–992

19 Mejean, V., Iobbinivol, C., Lepelletier, M., Giordano, G., Chippaux, M. and Pascal, M. C. (1994) TMAO anaerobic respiration in *Escherichia coli*: involvement of the *Tor* operon. Mol. Microbiol. **11**, 1169–1179

20 Jungst, A., Wakabayashi, S., Matsubara, H. and Zumft, W. G. (1991) The *nirSTBM* region coding for cytochrome-cd_1-dependent nitrite respiration of *Pseudomonas stutzeri* consists of a cluster of monoheme, diheme, and tetraheme proteins. FEBS Lett. **279**, 205–209

21 Simon, J., Gross, R., Einsle, O., Kroneck, P. M. H., Kroger, A. and Klimmek, O. (2000) A NapC/NirT-type cytochrome *c* (NrfH) is the mediator between the quinone pool and the cytochrome *c* nitrite reductase of *Wolinella succinogenes*. Mol. Microbiol. **35**, 686–696

22 Mouncey, N. J., Choudhary, M. and Kaplan, S. (1997) Characterization of genes encoding dimethyl sulfoxide reductase of *Rhodobacter sphaeroides* 2.4.1(T): an essential metabolic gene function encoded on chromosome II. J. Bacteriol. **179**, 7617–7624

23 Rosenbaum, M. A., Bar, H. Y., Beg, Q. K., Segre, D., Booth, J., Cotta, M. A. and Angenent, L. T. (2012) Transcriptional analysis of *Shewanella oneidensis* MR-1 with an electrode compared to Fe(III)citrate or oxygen as terminal electron acceptor. PLoS ONE **7**, e30827

24 Beliaev, A. S., Klingeman, D. M., Klappenbach, J. A., Wu, L., Romine, M. F., Tiedje, J. A., Nealson, K. H., Fredrickson, J. K. and Zhou, J. (2005) Global transcriptome analysis of *Shewanella oneidensis* MR-1 exposed to different terminal electron acceptors. J. Bacteriol. **187**, 7138–7145

25 Berks, B. C., Richardson, D. J., Robinson, C., Reilly, A., Aplin, R. T. and Ferguson, S. J. (1994) Purification and characterization of the periplasmic nitrate reductase from *Thiosphaera pantotropha*. Eur. J. Biochem. **220**, 117–124

26 Field, S. J., Dobbin, P. S., Cheesman, M. R., Watmough, N. J., Thomson, A. J. and Richardson, D. J. (2000) Purification and magneto-optical spectroscopic characterization of cytoplasmic membrane and outer membrane multiheme *c*-type cytochromes from *Shewanella frigidimarina* NCIMB400. J. Biol. Chem. **275**, 8515–8522

27 Kim, H. J., Zatsman, A., Upadhyay, A. K., Whittaker, M., Bergmann, D., Hendrich, M. P. and Hooper, A. B. (2008) Membrane tetraheme cytochrome cm_{552} of the ammonia-oxidizing *Nitrosomonas europaea*: a ubiquinone reductase. Biochemistry **47**, 6539–6551

28 Shaw, A. L., Hochkoeppler, A., Bonora, P., Zannoni, D., Hanson, G. R. and McEwan, A. G. (1999) Characterization of DorC from *Rhodobacter capsulatus*, a *c*-type cytochrome involved in electron transfer to dimethyl sulfoxide reductase. J. Biol. Inorg. Chem. **274**, 9911–9914

29 Schwalb, C., Chapman, S. K. and Reid, G. A. (2002) The membrane-bound tetrahaem *c*-type cytochrome CymA interacts directly with the soluble fumarate reductase in *Shewanella*. Biochem. Soc. Trans. **30**, 658–662

30 Firer-Sherwood, M., Pulcu, G. S. and Elliott, S. J. (2008) Electrochemical interrogations of the Mtr cytochromes from *Shewanella*: opening a potential window. J. Biol. Inorg. Chem. **13**, 849–854

31 Myers, C. R. and Myers, J. M. (1993) Role of menaquinone in the reduction of fumarate, nitrate, nitrite, iron(III) and manganese(IV) by *Shewanella putrefaciens* MR-1. FEMS Microbiol. Lett. **114**, 215–222

32 Akagawamatsushita, M., Itoh, T., Katayama, Y., Kuraishi, H. and Yamasato, K. (1992) Isoprenoid quinone composition of some marine *Alteromonas*, *Marinomonas*, *Deleya*, *Pseudomonas* and *Shewanella* species. J. Gen. Microbiol. **138**, 2275–2281

33 Dobbin, P. S., Butt, J. N., Powell, A. K., Reid, G. A. and Richardson, D. J. (1999) Characterization of a flavocytochrome that is induced during the anaerobic respiration of Fe^{3+} by *Shewanella frigidimarina* NCIMB400. Biochem. J. **342**, 439–448

34 Shi, L., Lin, J. T., Markillie, L. M., Squier, T. C. and Hooker, B. S. (2005) Overexpression of multi-heme *c*-type cytochromes. BioTechniques **38**, 297–299

35 Shi, L., Chen, B., Wang, Z., Elias, D. A., Mayer, M. U., Gorby, Y. A., Ni, S., Lower, B. H., Kennedy, D. W., Wunschel, D. S. et al. (2006) Isolation of a high-affinity functional protein complex between OmcA and MtrC: two outer membrane decaheme *c*-type cytochromes of *Shewanella oneidensis* MR-1. J. Bacteriol. **188**, 4705–4714

36 Berry, E. A. and Trumpower, B. L. (1987) Simultaneous determination of hemes-*a*, hemes-*b*, and hemes-*c* from pyridine hemochrome spectra. Anal. Biochem. **161**, 1–15

37 Okun, V. M., Lummen, P. and Brandt, U. (1999) Three classes of inhibitors share a common binding domain in mitochondrial complex I (NADH:ubiquinone oxidoreductase). J. Biol. Chem. **274**, 2626–2630

38 Marritt, S. J., Kemp, G. L., Xiaoe, L., Durrant, J. R., Cheesman, M. R. and Butt, J. N. (2008) Spectroelectrochemical characterization of a pentaheme cytochrome in solution and as electrocatalytically active films on nanocrystalline metal-oxide electrodes. J. Am. Chem. Soc. **130**, 8588–8589

39 Zargar, K. and Saltikov, C. W. (2009) Lysine-91 of the tetraheme *c*-type cytochrome CymA is essential for quinone interaction and arsenate respiration in *Shewanella* sp strain ANA–3. Arch. Microbiol. **191**, 797–806

40 Cheesman, M. R., Watmough, N. J., Gennis, R. B., Greenwood, C. and Thomson, A. J. (1994) Magnetic circular dichroism studies of *Escherichia coli* cytochrome *bo*: identification of high-spin ferric, low-spin ferric and ferryl [Fe(IV)] forms of heme-*o*. Eur. J. Biochem. **219**, 595–602

41 Thomson, A. J., Cheesman, M. R. and George, S. J. (1993) Variable-temperature magnetic circular-dichroism. Metallobiochemistry **226**, 199–232

42 Upadhyay, A. K., Petasis, D. T., Arciero, D. M., Hooper, A. B. and Hendrich, M. P. (2003) Spectroscopic characterization and assignment of reduction potentials in the tetraheme cytochrome c_{554} from *Nitrosomonas europaea*. J. Am. Chem. Soc. **125**, 1738–1747

43 Pereira, I. A. C., LeGall, J., Xavier, A. V. and Teixeira, M. (2000) Characterization of a heme *c* nitrite reductase from a non-ammonifying microorganism, *Desulfovibrio vulgaris* Hildenborough. Biochim. Biophys. Acta **1481**, 119–130

44 Pond, A. E., Sono, M., Elenkova, E. A., Goodin, D. B., English, A. M. and Dawson, J. H. (1999) Influence of protein environment on magnetic circular dichroism spectral properties of ferric and ferrous ligand complexes of yeast cytochrome *c* peroxidase. Biospectroscopy **5**, S42–S52

45 Marritt, S. J., van Wonderen, J. H., Cheesman, M. R. and Butt, J. N. (2006) Magnetic circular dichroism of hemoproteins with *in situ* control of electrochemical potential: 'MOTTLE'. Anal. Biochem. **359**, 79–83

46 Murphy, J. N. and Saltikov, C. W. (2007) The *cymA* gene, encoding a tetraheme *c*-type cytochrome, is required for arsenate respiration in *Shewanella* species. J. Bacteriol. **189**, 2283–2290

47 Kern, M., Einsle, O. and Simon, J. (2008) Variants of the tetrahaem cytochrome *c* quinol dehydrogenase NrfH characterize the menaquinol-binding site, the haem *c*-binding motifs and the transmembrane segment. Biochem. J. **414**, 73–79

48 Cartron, M. L., Roldan, M. D., Ferguson, S. J., Berks, B. C. and Richarson, D. J. (2002) Identification of two domains and distal histidine ligands to the four haems in the bacterial *c*-type cytochrome NapC; the prototype connector between quinol/quinone and periplasmic oxido-reductases. Biochem. J. **368**, 425–432

49 McMillan, D. G. G., Marritt, S. J., Butt, J. N. and Jeuken, L. J. C. (2012) Menaquinone-7 is a specific co-factor in the tetraheme quinol dehydrogenase CymA. J. Biol. Chem., **287**, 14215–14225

50 Firer-Sherwood, M. A., Bewley, K. D., Mock, J. Y. and Elliott, S. J. (2011) Tools for resolving complexity in the electron transfer networks of multiheme cytochromes *c*. Metallomics **3**, 344–348

Received 1 February 2012/12 March 2012; accepted 29 March 2012
Published as BJ Immediate Publication 29 March 2012, doi:10.1042/BJ20120197

Biochem. J. (2012) **444**, 465–474 (Printed in Great Britain) doi:10.1042/BJ20120197

online data

SUPPLEMENTARY ONLINE DATA

A functional description of CymA, an electron-transfer hub supporting anaerobic respiratory flexibility in *Shewanella*

Sophie J. MARRITT*, Thomas G. LOWE*, Jordan BYE*, Duncan G. G. McMILLAN†, Liang SHI‡, Jim FREDRICKSON‡, John ZACHARA‡, David J. RICHARDSON*, Myles R. CHEESMAN*, Lars J. C. JEUKEN† and Julea N. BUTT*[1]

*Centre for Molecular and Structural Biochemistry, School of Chemistry and School of Biological Sciences, University of East Anglia, Norwich NR4 7TJ, U.K., †Institute of Membrane and Systems Biology, Centre for Molecular Nanoscience, School of Physics and Astronomy, University of Leeds, Leeds LS2 9JT, U.K., and ‡Pacific Northwest National Laboratory, Richland, WA 99352, U.S.A.

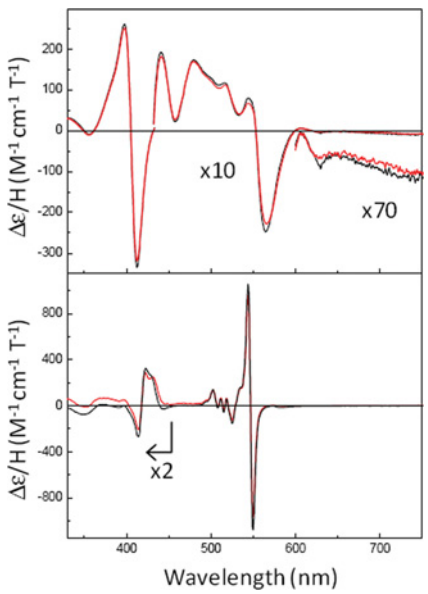

Figure S1 The ambient temperature MCD for CymA in the presence of HQNO

The spectra shown in red are for CymA with a 20-fold excess of HQNO and the spectra shown in black are CymA without added HQNO. Upper panel, isolated 20 μM CymA; bottom panel, 10 μM CymA fully reduced with dithionite. The buffer conditions were 20 mM Hepes (pH 7) containing approximately 0.05 % DDM.

Table S1 MALDI–TOF-MS analysis of tryptic digests of CymA

Listed are the predicted peptides of trypsin-digested CymA which would not contain covalently bound haem and are of detectable size by MALDI–TOF-MS. A total of three out of the four peptides were detected in the excised SDS/PAGE gel band at 24 kDa. The most intense absorption at mass 1806.9 Da was detected in excised gel bands at 24 kDa and 50 kDa.

Residues in CymA	Predicted tryptic digest	Theoretical mass (Da) $[M + H]^+$	MALDI mass (m/z)
97–118	DLYGFLTIDGFNTQAWLDENRK	2616.27	2616.28
193–209 (V5 tag)	LEGKPIPNPLLGLDSTR	1820.03	1820.05
143–157	IYENQPETMKPMAVR	1806.89	1806.9
57–68	NEVLASAHGGGK	1139.58	Not detected

Received 1 February 2012/12 March 2012; accepted 29 March 2012
Published as BJ Immediate Publication 29 March 2012, doi:10.1042/BJ20120197

[1] To whom correspondence should be addressed (email j.butt@uea.ac.uk).